Materials Science and Engineering C 60 (2016) 285–292

Contents lists available at ScienceDirect

Materials Science and Engineering C

journal homepage: www.elsevier.com/locate/msec

# Development of dental composites with reactive fillers that promote precipitation of antibacterial-hydroxyapatite layers

Anas Aljabo [a], Ensanya A. Abou Neel [a,b,c], Jonathan C. Knowles [a], Anne M. Young [a,*]

[a] UCL Eastman Dental Institute, Biomaterials & Tissue Engineering Division, 256 Gray's Inn Road, London WC1X 8LD, United Kingdom
[b] Division of Biomaterials, Operative Dentistry Department, Faculty of Dentistry, King Abdulaziz University, Jeddah, Saudi Arabia
[c] Biomaterials Department, Faculty of Dentistry, Tanta University, Tanta, Egypt

ARTICLE INFO

*Article history:*
Received 26 February 2015
Received in revised form 23 October 2015
Accepted 16 November 2015
Available online 18 November 2015

*Keywords:*
Dental composite
Mono- and tricalcium phosphate
Antibacterial
Hydroxyapatite precipitation

ABSTRACT

The study aim was to develop light-curable, high strength dental composites that would release calcium phosphate and chlorhexidine (CHX) but additionally promote surface hydroxyapatite/CHX co-precipitation in simulated body fluid (SBF). 80 wt.% urethane dimethacrylate based liquid was mixed with glass fillers containing 10 wt.% CHX and 0, 10, 20 or 40 wt.% reactive mono- and tricalcium phosphate (CaP). Surface hydroxyapatite layer thickness/coverage from SEM images, Ca/Si ratio from EDX and hydroxyapatite Raman peak intensities were all proportional to both time in SBF and CaP wt.% in the filler. Hydroxyapatite was, however, difficult to detect by XRD until 4 weeks. XRD peak width and SEM images suggested this was due to the very small size (~10 nm) of the hydroxyapatite crystallites. Precipitate mass at 12 weeks was 22 wt.% of the sample CaP total mass irrespective of CaP wt.% and up to 7 wt.% of the specimen. Early diffusion controlled CHX release, assessed by UV spectrometry, was proportional to CaP and twice as fast in water compared with SBF. After 1 week, CHX continued to diffuse into water but in SBF, became entrapped within the precipitating hydroxyapatite layer. At 12 weeks CHX formed 5 to 15% of the HA layer with 10 to 40 wt.% CaP respectively. Despite linear decline of strength and modulus in 4 weeks from 160 to 101 MPa and 4 to 2.4 GPa, respectively, upon raising CaP content, all values were still within the range expected for commercial composites. The high strength, hydroxyapatite precipitation and surface antibacterial accumulation should reduce tooth restoration failure due to fracture, aid demineralised dentine repair and prevent subsurface carious disease respectively.



## 1. Introduction

Dental composites have been used for over 50 years as restorative materials [1]. Compared to dental amalgam, they trigger less safety concerns and provide improved aesthetics. Over the years there has been a significant increase in mechanical properties of commercial resin-based filling composites enabling a reduction in failure due to fracture and wear. Polymerisation shrinkage and lack of anti-bacterial activity, however, are continuing issues as they enable micro-gap formation between the tooth and restoration followed by bacterial microleakage. These bacteria can cause continuing disease and de-mineralisation of dentine underneath a restoration. Subsequent action by matrix metalloproteinases (MMPs) then degrades the demineralised dentinal collagen further widening the micro-gap. Recurrent caries is now the major reason for the shorter median survival lifespan (5–6 year) of composites in comparison with more antibacterial dental amalgam (13 years) [1–4]. Dental composites are typically composed of four major components: an organic polymer matrix (produced from dimethacrylate monomers such as UDMA, BisGMA, TEGDMA), inorganic fillers (e.g. glass, ceramic), coupling agents and the initiator–accelerator system. Much work has focussed upon varying these components to reduce shrinkage and improve mechanical properties [5–8]. To prevent bacterial microleakage, however, new components are additionally required to promote remineralisation (e.g. through calcium and phosphate release) and antibacterial action.

In the past 20 years a wide range of calcium phosphates (CaP) such as hydroxyapatite (HA) [9–11], amorphous calcium phosphates (ACP) [12–15], tetracalcium phosphate (TTCP) [16] and mono- and dicalcium phosphates (MCPM and DCPA) [17–19] have been studied as fillers in an attempt to produce calcium and phosphate — releasing dental composites. Both nano-sized and micro-sized HA particles have been investigated with the latter tending to give higher mechanical properties [9,17]. Acidic coupling agent optimisation could improve flexural strength but a maximum of only ~70 MPa was achieved [9,10]. ACP filled composites were shown to release calcium and phosphate at levels dependent upon the amount added to the formulations [20]. The biaxial flexural strength could be increased to ~75 MPa through hybridisation of the ACP with other elements (e.g. silicon and zirconium) but was still generally half that for base resin [13–15,21]. Initial low strengths

* Corresponding author at: 139, UCL Eastman Dental Institute, 256 Gray's Inn Road, London WC1X 8LD, United Kingdom.

http://dx.doi.org/10.1016/j.msec.2015.11.047

could be attributed in part to poor dispersion and insufficient interaction between ACP and resin but might also be caused by the generation of pores upon component release and increased water sorption after water storage. The strength of TTCP filled composites was increased from ~50 to 100 MPa upon replacing 50% of the TTCP by silicon nitride whiskers. Calcium and phosphate release, however, was decreased by an order of magnitude [16]. Similar effects were observed with MCPM/whisker composites [17]. Replacing MCPM with less soluble DCPA increased strength but drastically reduced calcium phosphate release [17,20]. Furthermore, the addition of whiskers compromised optical properties preventing light cure feasibility.

More recently, reactive acidic and basic mono- and tricalcium phosphate fillers (MCPM/β-TCP) have been added together in dental composites [22]. The β-TCP enabled more control over the MCPM dissolution and composite water sorption. Highly soluble MCPM on the surface of the material dissolved but in the bulk it reacted with the β-TCP to form less soluble, water-binding brushite (dicalcium phosphate dihydrate) crystals. The strengths of these composites were subsequently improved through partial replacement of the reactive fillers with reinforcing fillers but these again compromised optical properties [23].

In the above studies, remineralisation potential was generally assessed through calcium and phosphate release determination [24]. Predicting the release levels required to promote remineralisation, however, is complex and dependent upon many other parameters. A dental restoration that promotes HA deposition could in addition to providing remineralisation of adjacent collagen, potentially also enable closure of gaps between the material and tooth and reduce bond deterioration over time. In this study, therefore, remineralisation potential was evaluated through calcium and phosphate release and their precipitation as HA layer on the surface. Some dental Portland cements, adhesives and ceramics have shown hydroxyapatite precipitates on their surfaces in simulated body fluids (SBF) [25–28]. In one study it was shown they could also re-mineralise adjacent human dentin [28].

Factors increasing rates of HA precipitation on the surface of a material include raised SBF supersaturation, pH and temperature. Material surface chemistry has also been shown to be important (e.g. by providing nucleation sites) [29–32]. In these studies, SEM, EDX, Raman, FTIR and XRD have all been employed to assess the hydroxyapatite precipitates. These studies, however, were largely only semi-quantitative. In addition material mass changes have been monitored to provide quantitative results. Such gravimetric methods are complicated in composites studies, however, because of large composite changes in mass upon water sorption and component release.

To provide anti-bacterial action, various agents including fluoride [20,33] and chlorhexidine (CHX) [15,34] have been added to composites. There is conflicting evidence over whether the addition of fluoride in commercial composites has any clinical benefit [24,35]. CHX was added into various experimental dental composites due its low minimum inhibitory concentrations against oral bacteria and ability to inhibit MMPs [34,36]. Composites with early release of chlorhexidine might reduce the need for extensive caries affected tissue removal as advocated in modern tooth restoration procedures [37]. The CHX, however, is not readily released from the bulk of conventional composites. This problem has been solved through combining CHX with reactive MCPM/β-TCP [23].

The aim of this study was therefore to develop methods that provide a quantitative assessment of any hydroxyapatite layer on the surfaces of systematically varying new MCPM, β-TCP and CHX-containing light curable composites. In addition, this study will assess if these new materials also have high CHX release and enhanced mechanical strengths. The precipitated HA-CHX layer was thoroughly investigated to provide a deep understanding to factors that determines precipitation kinetics. This study not only aims to form interactive composites that promote precipitation of HA-CHX layer, but also provides a detailed explanation to the nature of the precipitated layer and how it was formed. Furthermore, it is known that hydroxyapatite can promote the precipitation of chlorhexidine from solution [38]. This study will therefore address, how the formation of the HA layer affects the release of CHX and whether any of this antibacterial can be entrapped with the HA to potentially enable a long-term antibacterial restoration/dentine interface.

## 2. Materials and methods

### 2.1. Composite paste preparation

In this study, urethane dimethacrylate (UDMA, Esstech) was used as the base monomer. Triethylene glycol dimethacrylate (TEGDMA, Esstech) and hydroxyethyl methacrylate (HEMA, Esstech) were added as diluents and camphorquinone (CQ, Sigma-Aldrich)/dimethylparatoluidine (DMPT, Sigma-Aldrich) as initiator/activator respectively. UDMA:TEGDMA: HEMA:CQ: DMPT was 68:25:5:1:1 by weight.

The composite filler consisted of radiopaque barium–alumino–silicate glass with an average particle diameter of 7 μm (1 to 20 μm diameter range by SEM) (DMG, Hamburg, Germany). Its refractive index (0.52) matched well that of the monomer phase (0.48) to enable good depth of cure. Chlorhexidine diacetate salt hydrate (CHX, Sigma-Aldrich) and borosilicate glass fibres (15 μm diameter × 300 μm length) (MO-SCI Healthcare L.L.C. Rolla, USA) levels were fixed at 20 and 10 wt.% of the total filler respectively. Reactive calcium phosphate (CaP, equal masses of β-tricalcium phosphate (β-TCP, Plasma Biotal) and monocalcium phosphate monohydrate (MCPM, Himed)) levels were 0, 10, 20 or 40 weight % (wt.%) of the filler. The base powder phase therefore contributed 30, 50, 60 or 70 wt.% of the filler. Powder and liquid phases were combined at a ratio of 4:1.

### 2.2. Composite disc preparation

To prepare disc-shaped specimens, pastes were placed in metal rings (1 mm deep and 10 mm internal diameter), covered top and bottom with acetate sheet and light cured with blue light (Demi Plus, Kerr) with 1100 mW/cm$^2$ output for 40 s top and bottom. This long cure time ensures maximum polymerisation of the whole disc and greater than 70% conversion irrespective of formulation as assessed by FTIR. The resultant composite discs were removed from the moulds and their edges polished with 1000 grit paper to remove any loose chips. They were subsequently stored dry in sterilin tubes overnight before testing or immersion either in water or a simulated body fluid (SBF) (as in ISO 23317:2007).

### 2.3. Characterisation of hydroxyapatite deposition

The morphology, elemental composition, chemical changes, crystallinity and mass of any deposited layer on the surface of composites were assessed after immersion in 10 ml of water or SBF for periods ranging from 1 day up to 12 weeks using the techniques below. During the storage periods the solutions were left unchanged to mimic accumulation of components as might occur underneath a sealed tooth restoration.

#### 2.3.1. Scanning electron microscopy and energy dispersive X-ray analysis

To assess the morphology and elemental composition of the precipitated layer, scanning electron microscopy (SEM) with energy dispersive X-ray (EDX) analysis was employed. Specimens stored for 1 day or 1, 2, 3, 4 and 8 weeks were mounted onto stubs with fast setting epoxy adhesive. The mounted specimens were then sputter coated using gold and palladium alloy. All SEM images were captured at 5 kV accelerating voltage using a Scanning electron microscope (Phillip XL-30, Eindhoven, The Netherlands) and INCA software.

EDX analysis was performed using an Inca X-sight 6650 detector (Oxford Instrument, UK) at 20 kV accelerating voltage to quantify the average and homogeneity of calcium versus silicon content of the

surfaces. The surface of the composite was divided into 9 squares each $3 \times 3$ mm$^2$, ignoring the 1 mm edge area which could be contaminated with the epoxy resin. Acquisition time to map each square was 200 s with a Count Rate Optimisation process time of 6. Ca/P ratio was determined to first confirm HA formation. Subsequently, the ratio of Ca from HA to Si in the glass filler, was used to investigate relative changes in the thickness/homogeneity of the HA layer with time and composite composition.

*2.3.2. Raman*

Raman spectroscopy was utilised to further quantify any surface changes and hydroxyapatite formation after 1 day, or 1, 2 and 4 weeks. All spectra were obtained using a Lab Ram spectrometer (Horiba, Jobin Yvom, France). The samples were excited at 633 nm by a He–Ne laser through a microscope objective (50×). Raman spectra were obtained in the range of 850–1700 cm$^{-1}$ with a resolution 2 cm$^{-1}$ using a confocal hole of 150 μm. For each specimen, spectra were obtained by mapping areas of $40 \times 40$ μm. For each area ($n = 3$), several hundreds of spectra were generated and normalised using data between 1200 and 1700 cm$^{-1}$ prior to obtaining average spectra. To aid peak assignment, spectra were generated for pure β-TCP, MCPM, CHX and glass as well as the polymerised monomer.

*2.3.3. X-ray diffraction*

Surface X-ray diffraction (XRD) (thin film) spectra of samples stored for 1, 2, 3 or 4 weeks in water or SBF were obtained using a Bruker-D8 Advance Diffractometer (Brüker, UK) using Ni filtered Cu Kα radiation. Data were collected using a Scintillation counter with a step size of 0.02° over an angular range of 20–55° 2Θ and a count time of 10 s. The width of the XRD peak was used to estimate the size of the HA crystals [39] using the Scherrer Eq. (1):

$$\tau = \frac{K\lambda}{\beta \cos\Theta} \tag{1}$$

$\tau$ is the mean size of HA crystals, K is dimensionless shape factor ~0.9, λ is the X-ray wavelength = 0.15 nm, $\beta$ is the line broadening at half the maximum intensity and $\Theta$ is the Bragg angle.

*2.3.4. Mass of HA*

To determine the mass of HA on the surface of specimens stored for 12 weeks in SBF, the HA layer was very carefully scraped off using a metal blade and assessed gravimetrically. Sample repetition for each formulation was 3.

*2.4. Chlorhexidine release and entrapment in HA layer*

To quantify CHX release, discs of each composition ($n = 3$) were weighed and immersed in 10 ml of distilled water or SBF (at 37 °C) within sterile tubes. At various time points up to 12 weeks (2, 4, 6, 24, 168, 336, 720, 1440 and 2160 h), the specimens were removed and replaced in fresh distilled water or SBF. UV spectra of storage solutions were obtained between 190 and 300 nm using a UV 500 spectrometer (Thermo Spectronic, UK). These were compared with calibration graphs created in the same range for solutions of known concentration of CHX to ensure that the CHX was the only component causing absorbance. The CHX peak at 255 nm was then used to calculate the amount of CHX release ($R_t$ in grammes) between different time periods from each specimen using Eq. (2):

$$R_t = \frac{A}{g} V \tag{2}$$

Where A is the absorbance at 255 nm, g is the gradient of a calibration curve of absorbance vs CHX concentration (obtained using known solutions) and V is the storage solution volume. The percentage cumulative amount of drug release $R_c$ at time t was then given by Eq. (3):

$$R_C(\%) = \frac{100\left[\sum_0^t R_t\right]}{W_c} \tag{3}$$

$W_c$ is the weight of CHX incorporated in a given specimen in grammes.

To assess the level of CHX deposited/trapped in the surface hydroxyapatite layers after 12 weeks in SBF, the HA from the test in Section 2.3.4 was dissolved in 10 ml of deionised water. This was achieved by mixing for 24 h using a small stirrer. The UV spectra of the resultant solutions were then obtained.

*2.5. Biaxial flexural strength and modulus*

To assess strength and modulus, discs of each formulation ($n = 6$) were prepared as above and stored for 1 month in SBF. Biaxial flexural strength, S, and modulus, E, were determined using a "ball on ring" jig and a universal testing machine (Instron 4502, UK) with Eqs. (4) and (5)

$$S = \frac{P}{h^2}\left[(1+\mu)\left(0.485 \ln\left(\frac{a}{h}\right) + 0.52\right) + 0.48\right] \tag{4}$$

$$E = 0.502 \frac{dP}{dw}\left(\frac{a^2}{h^3}\right) \tag{5}$$

(P, load (N); h, sample thickness (mm); μ, Poisons ratio taken as 0.3; dP/dw, the gradient of load versus central deflection; a, the support radius (mm)).

*2.6. Linear regression analysis and 95% confidence intervals*

The function Linest in Microsoft excel was used to fit linear equations to average properties versus variables. This function provided standard errors on gradients and intercepts and $R^2$ values. 95% confidence intervals were estimated assuming they were 2 times standard errors. These are provided as error bars on graphs (unless mentioned otherwise as in Fig. 2) and in parentheses with equations. Linest was first applied assuming a non-zero intercept. If the intercept was smaller than its estimated 95% confidence interval, the analysis was repeated assuming a zero intercept.

## 3. Results

*3.1. Characterisation of hydroxyapatite formation*

*3.1.1. Scanning electron microscopy*

SEM images of any composites stored dry or in water showed only scratches and small pores (e.g. Fig. 1a). Any samples containing CaP and stored in SBF for one day or more, however, were covered with HA spheres (Fig. 1b–d). From SEM it was noticeable that the percentage of the surface covered by HA and the average size of the HA spheres increased with raised CaP content in the samples or time in SBF. At early times the layers were just 1 sphere thick. At later times, however, the HA precipitate consisted of larger, aggregating and/or multiple layers of spheres. After 4, 2 and 1 week, in SBF, samples containing 10, 20 and 40% CaP were approximately 90% covered with HA respectively. At high magnification the spheres had a sponge like appearance with pores of approximately 100 nm diameter. The pore walls were approximately 10 nm thick (Fig. 1e and f). Upon very close inspection the walls appeared to consist of balls of approximately 10 nm diameter.

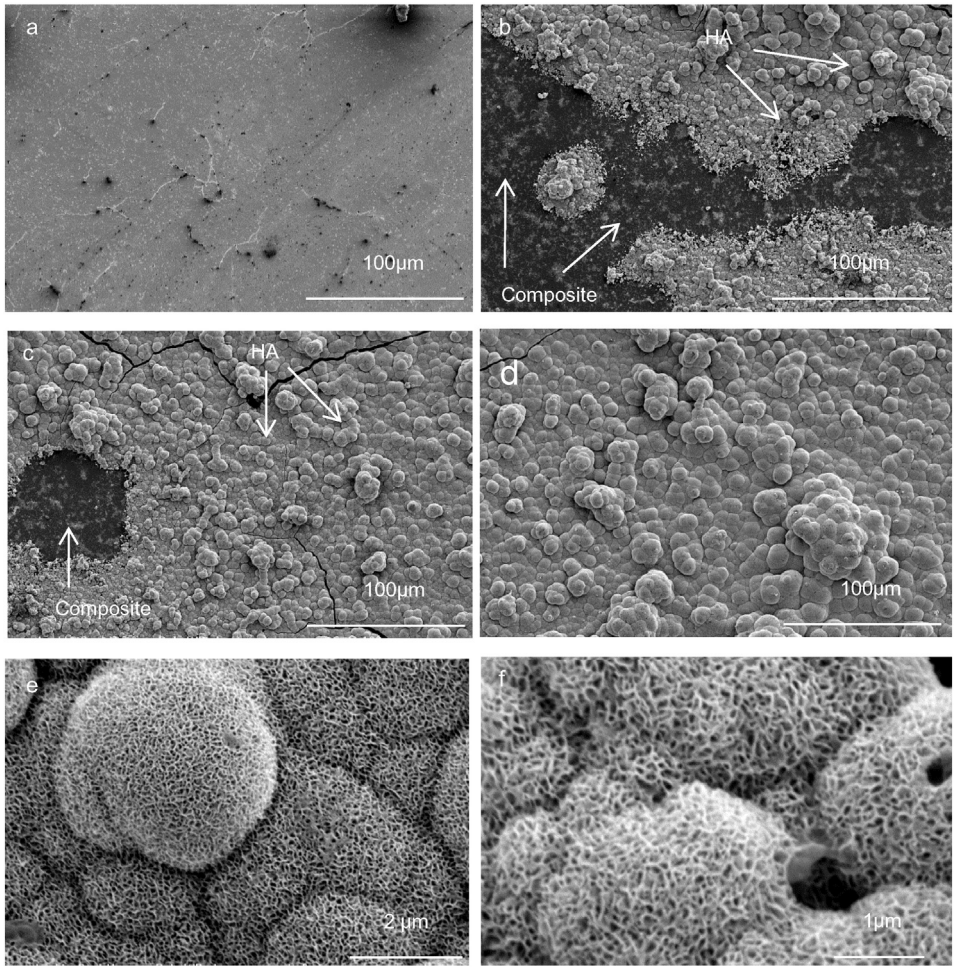


**Fig. 1.** SEM images for composite (a) 0% CaP, (b) 10% CaP, (c, e and f) 20% CaP and (d) 40% CaP immersed in SBF for 1 week.

*3.1.2. EDX*

From EDX the ratio of Ca/P in the precipitate was 1.67 when focussed solely upon the precipitate as expected for HA. When examining the composite surface it could be 0, 0.5 or 1.5 dependent upon whether glass/polymer, MCPM or TCP was being observed respectively. Full surface mapping of the composite surfaces showed that the ratio of Ca (primarily from HA) to Si (in the composite glass) increased linearly with storage time in SBF between 1 and 30 days (Fig. 2). The gradients were also proportional to the calcium phosphate content (see Table 1).

The error bars in Fig. 2 provide an indication of the level of HA variation in thickness across the sample. When the stdev error bars at later times do not overlap significantly with the initial error bars the surfaces are fully covered with HA layer. This occurs at 1, 3 and >4 weeks with 40, 20 and 10% CaP respectively.

*3.1.3. Raman*

*3.1.3.1. Monitoring HA formation.* Example average Raman spectra before and after immersion in SBF are illustrated in Fig. 3a. For the dry surface, various sharp CHX peaks are observed including one at 1600 $cm^{-1}$. Additionally a glass peak at 1400 $cm^{-1}$ and polymer peaks at 1445, 1640 and 1718 $cm^{-1}$ were evident. Phosphate peaks (P–O stretch) at 901, 912 and 1108 $cm^{-1}$ due to MCPM, and 943 and 968 $cm^{-1}$ for β-TCP were also present. After 1 week immersion in SBF or water, the peaks attributed to MCPM disappeared. Those due to β-TCP remained after water immersion but were masked by the very intense HA peak at 960 $cm^{-1}$ for composites immersed in SBF.

*3.1.3.2. Monitoring HA growth.* Normalised average Raman spectra of composite samples indicated that the intensity of the HA peaks increased linearly with both CaP content and time of immersion in SBF (Fig. 3b and c). The gradients of HA normalised intensity versus time was also proportional to CaP content (see linear regression parameters in Table 1).

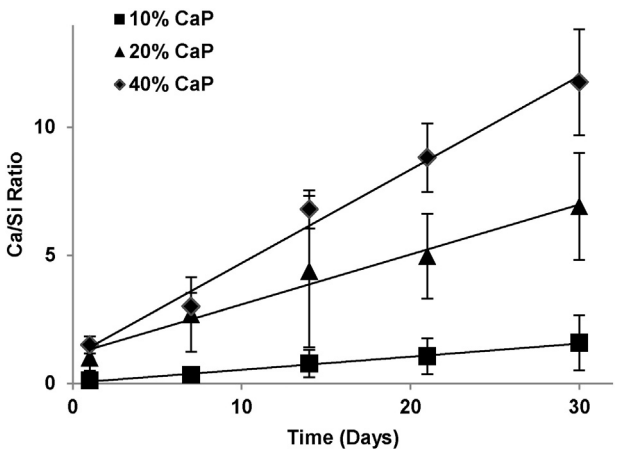


**Fig. 2.** The average Ca: Si ratio on the surfaces of different formulations (10, 20 and 40% CaP), after 1, 7, 14, 21 and 30 days in SBF. Error bars (stdev with n = 9 areas) indicate the layer homogeneity on a single specimen. Each point is a different specimen.

**Table 1**
Gradients of Ca/Si ratio and normalised 980 $cm^{-1}$ peak versus time from EDX and Raman respectively, mass of surface hydroxyapatite at 12 weeks, gradient of CHX release versus the square root of time in water and SBF, CHX entrapment in the HA layer at 12 weeks and 4 week flexural strength and modulus results for formulations with 0, 10, 20 and 40% CaP. Gradients and intercepts of the data versus CaP wt.% are also provided with $R^2$ values at the bottom of each column. Errors represent 95% CI.

| CaP (wt.% of filler) | Ca/Si vs t (mol/mol $day^{-1}$) | Raman HA peak intensity $day^{-1}$ | HA at 12 weeks (% of specimen) | CHX release vs sqrt t (%/$h^{0.5}$) water | CHX release vs sqrt t (%/$h^{0.5}$) SBF | CHX in HA layer (% of total CHX) | Flexural strength (MPa) | Flexural modulus (GPa) |
|---|---|---|---|---|---|---|---|---|
| 0 | 0.00 ± 0.01 | 0.0 ± 0.0 | 0.0 ± 0.0 | 0.00 ± 0.01 | 0.00 ± 0.01 | 0.00 ± 0.01 | 160 ± 8 | 4.0 ± 0.2 |
| 10 | 0.05 ± 0.00 | 15 ± 3 | 1.7 ± 0.3 | 0.10 ± 0.01 | 0.10 ± 0.02 | 1.0 ± 0.1 | 145 ± 5 | 3.6 ± 0.1 |
| 20 | 0.24 ± 0.03 | 36 ± 9 | 3.0 ± 0.1 | 0.28 ± 0.02 | 0.18 ± 0.01 | 4.9 ± 0.7 | 129 ± 4 | 3.2 ± 0.2 |
| 40 | 0.41 ± 0.03 | 66 ± 9 | 7.1 ± 1.7 | 0.61 ± 0.04 | 0.27 ± 0.4 | 13.6 ± 1.3 | 101 ± 8 | 2.4 ± 0.3 |
| Gradient | 0.010 ± 0.002 | 1.7 ± 0.1 | 0.17 ± 0.02 | 0.015 ± 0.001 | 0.007 ± 0.001 | 0.42 ± 0.03 | −1.47 ± 0.03 | −0.04 ± 0.001 |
| Intercept | 0 | 0 | 0 | 0 | 0 | 0 | 160 ± 2 | 4 ± 0.01 |
| $R^2$ | 0.98 | 0.99 | 0.99 | 0.99 | 0.98 | 0.99 | 0.99 | 1.00 |

### 3.1.4. XRD

XRD patterns of the 0 CaP sample and all other formulations immersed in water up to 1 month showed no HA peaks. Formulations 10, 20 and 40 CaP stored in SBF, however, showed low-crystallinity peaks appearing at about 26° and 32° 2Θ (Fig. 4). These were assigned as apatite on the basis of JCPDS Card 09-0432. The size of the crystals was estimated from the Scherrer equation to be ~10 nm.

### 3.1.5. HA layer mass

The average mass of the discs was 200 mg. The total mass of HA scrapped from the disc surfaces at 12 weeks was between 3 and 15 mg. This is provided in Table 1 as a percentage of the sample mass in addition to results from linear regression. These data show that the level of HA at this time was proportional to the calcium phosphate concentration in the samples.

### 3.2. CHX release in water vs SBF

The level of CHX release in water was proportional to the square root of time as expected for a diffusion controlled process (Fig. 5a). In SBF, the CHX release was linear versus $t^{0.5}$ only up to 1 week and began to plateau after this time (Fig. 5b). The early gradients are provided in Table 1. Linear regression shows these gradients are proportional to the calcium phosphate contents but in addition doubled in water compared to that in SBF.

The CHX trapped in the HA layer after 12 weeks in SBF was also proportional to the calcium phosphate content in the samples (see Table 1). From this data the concentration of CHX in these layers was calculated to be 5, 12 and 15 wt.% with 10, 20 and 40 wt.% CaP respectively. CHX in HA plus that released in SBF (3.3, 8.5, 18 wt.% with 10, 20 and 40 wt.% CaP respectively) was found to be approximately 2/3rd of the CHX released in water (4.2, 12, 27 wt.%).

### 3.3. Flexural strength and modulus

Biaxial flexural strength and modulus both decreased linearly with raising CaP level after storing for 1 month in SBF (see Table 1). The formulation with no CaP showed the highest flexural strength and modulus (160 MPa and 4 GPa respectively). Upon CaP addition, strength and modulus was reduced to 145 MPa and 3.6 GPa respectively for 10 CaP% formulation. Strength and modulus both continued to decrease with further increase in CaP, reaching 101 MPa and 2.4 GPa respectively for the 40% CaP formulation.

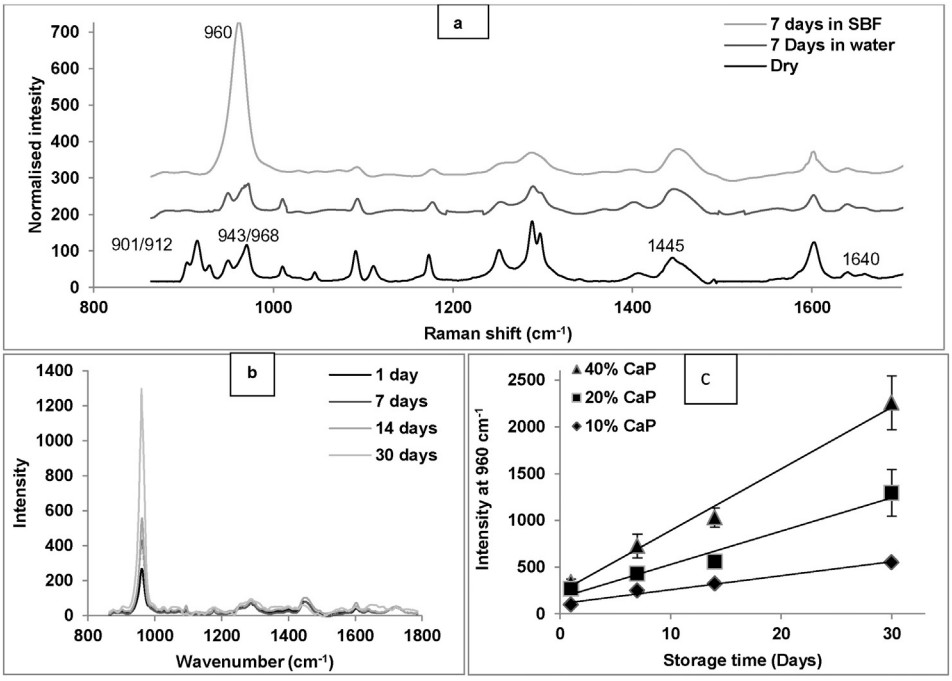


**Fig. 3.** Raman spectra for (a) composite with 20% CaP dry, 7 days in water and 7 days in SBF. (b) Raman spectra for composite with 20% CaP at 1, 7, 14 and 30 days of immersion in SBF. (c) Average intensity at 960 $cm^{-1}$ for 10, 20 and 40% CaP formulations plotted against time at 1, 7, 14 and 30 days (each point is for a different specimen. Error bars (n = 5) are stdev obtained from 5 spectra on a single specimen).

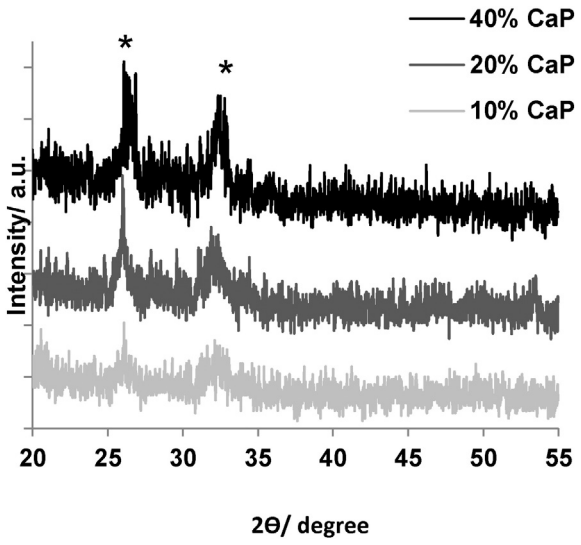


**Fig. 4.** XRD patterns for the 10, 20 and 40% CaP composite surfaces after storage in SBF for 1 month. Stars (*) indicate HA peaks.

## 4. Discussion

The above study has developed new quantitative methods of providing a detailed description of the morphology and density/thickness of HA precipitate on the surface of light cured composites, as a function of time in SBF. HA precipitations were shown to slow CHX release and trap this antibacterial within the hydroxyapatite layer. Even with high levels of reactive calcium phosphate these materials were shown to still have high flexural strength after 4 weeks immersion in SBF.

### 4.1. Characterisation of hydroxyapatite formation

Utilising SBF as a storage medium for both dental [6,14,40] and other medical devices is popular mainly due to the intensive investigation and development carried out to optimise SBF composition in the past decade [41], leading to the introduction of BS ISO 23317:2007 standard. Unlike the above new work this standard method and many previous studies, however, have limited their analysis to qualitative rather than quantitative assessment of precipitation kinetics [29,31,32].

The morphology of HA crystals shown by SEM images (Fig. 1) was comparable to that observed in previous studies using the standard method [39,41,42]. Other studies have shown that with reactive filler composites [22] monocalcium phosphate dissolves from the surface of the material in the first 24 h after placement in water. Subsequently, release of calcium and phosphate is much lower but the ratio of Ca/P higher [22]. This suggests that the early release is required to supersaturate the SBF and initiate the precipitation process. Other investigations showed composites with TCP or MCPM formed either no precipitate or brushite respectively on their surface in SBF (unpublished results). As pH decreases, the solubility of hydroxyapatite increases. Below pH ~ 4 the stable form of calcium phosphate in water is brushite and therefore precipitates instead [43]. A possible explanation of why hydroxyapatite forms instead of brushite when MCPM, TCP and CHX are present in the composites is therefore that the TCP and CHX may help to buffer the solutions in addition to providing the extra calcium required.

Using EDX it was possible to confirm that the precipitate had the correct Ca/P ratio for hydroxyapatite. By mapping relatively large areas ($3 \times 3$ mm$^2$), it was additionally possible to gain values for Ca/Si that provided a quantitative assessment of the level of precipitation. This ratio was low at early times because the layer was patchy and areas of uncovered composite were being observed. Once the composite was covered, silicon would still be detectable if the layer was thin and low density. As the thickness and density of the layer then increased detectable silicon would further declined. The increase in Ca/Si ratio with time and CaP content was therefore consistent with SEM images indicating increasing coverage, thickness and density of hydroxyapatite.

The dissolution of surface MCPM but not TCP upon composite placement in water observed above by Raman is consistent with much greater solubility of the former [41]. It is also in agreement with previous ion release studies from reactive filler composite [22]. The observation of a strong hydroxyapatite peak and its linear increase with time relative to composite surface peaks and CaP level are entirely consistent with the EDX data. As with EDX, the method of Raman analysis employed is expected to give a parameter that is sensitive to increasing coverage, thickness and density of hydroxyapatite. It is not surprising therefore that there is direct correlation between the Raman and EDX results.

The BS ISO 23317:2007 standard suggests samples should be stored for 4 weeks before analysis by XRD. Both EDX and Raman enabled detailed quantification of HA precipitation from day 1 in SBF up to 1 month. XRD was less sensitive to this process and unable to detect HA before 1 month presumably because the crystallite size was very small causing any peaks to be too broad to detect. Comparison of the EDX and XRD studies suggests the latter cannot detect the HA until the Ca/Si ratio exceeds 3. The XRD peaks at 26 and 32 2Θ were as expected for precipitated HA crystals with no heat treatment [44]. The width of the peak was consistent with a crystal size of comparable dimension to the smallest crystal balls observed by detailed examination of the high magnification SEM images.

As the samples above weigh 200 mg they will contain ~11 μmoles of calcium and phosphorus per weight percent of CaP in the filler phase. For the 10 and 40 wt.% CaP samples there is therefore ~110 and 450 μmoles of both calcium and phosphorus respectively. Formulations with 10 or more wt.% CaP will therefore contain much higher levels of

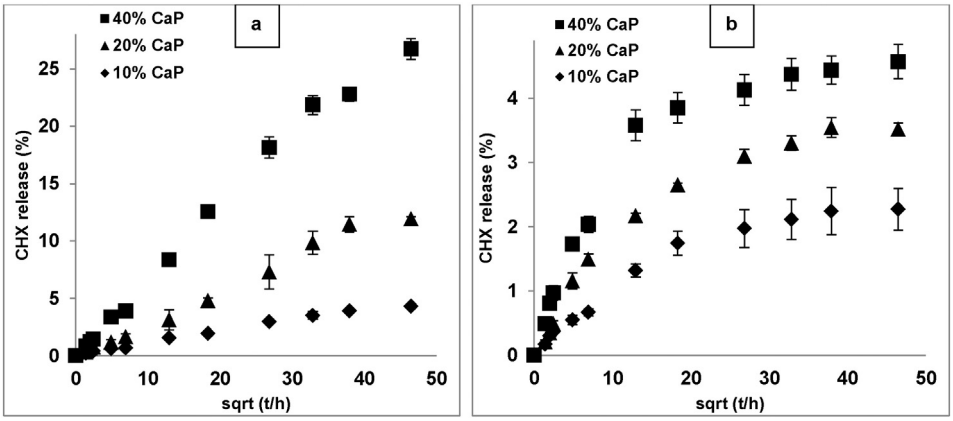


**Fig. 5.** CHX release versus the square root of time in water (a) and SBF (b) from 10, 20 and 40% CaP formulations up to 12 weeks.

these elements than in the 10 ml of SBF (10 and 25 μmoles of phosphorus and calcium respectively). Most of the ions forming the hydroxyapatite are therefore likely to be from the material rather than the SBF. 1 mg of hydroxyapatite contains 6 and 10 μmoles of phosphorus and calcium. Upon raising the CaP content from 10 to 40% the maximum mass of hydroxyapatite that might then be expected would therefore be from 11 to 45 mg. The mass percentages of HA observed on the material surfaces in Table 1 suggests that in 12 weeks 22% of the calcium phosphate from the sample had been released and reprecipitated on the surface. From the SEM images the highly porous HA precipitate would be expected to have a density ~¼ of that of the disc. The percentages of HA in Table 1 would then correspond with layers of ~30, 60 and 140 μm thickness at 12 weeks in agreement with SEM images.

### 4.2. CHX release in water vs SBF

CHX particles have been incorporated into dental restorative materials in previous studies for their antibacterial properties [34,45,46]. Recent studies showed that even small CHX release (2%) significantly reduced acidogenic bacterial counts (such as *Streptococcus mutans*), biofilm viability, biofilm formation, biofilm metabolic activity and lactic acid production [47,48]. Previous work showed restorations that release CHX can potentially kill bacteria in surrounding media in the first 4 weeks. After that the CHX release was exhausted and biofilms were then formed [47]. In this study, however, most of the CHX release was restricted where it was needed; at the composite surface within the precipitating HA layer. In addition, it is anticipated that if this layer is damaged and subsequently infiltrated by carious bacteria the acid they produce will dissolve the HA and release the antibacterial. The surface therefore responds to attack.

Early release of CHX from the experimental formulations in water was proportional to the sqrt of time, as expected for a diffusion controlled process (Fig. 5a). Increasing the CaP content substantially enhanced the release of CHX, which is in good agreement with a previous study [22]. This was attributed to increased water sorption induced by the CaP in the samples. This absorbed water dissolves the solid CHX enabling its release to the surrounding environment. In SBF, CHX released from the material was largely entrapped in the HA layer. Total CHX diffusion from the discs may have been lower in SBF than in water due to the higher ions concentration in SBF than water. These reduce the osmotic pressure difference leading to lower water sorption. A reduction in both water sorption and chlorhexidine release into phosphate buffer compared with water was previously observed [22].

From the mass of HA and percentage of CHX (Table 1) in this layer as the CHX make up 8 wt.% of the specimen, the level of CHX in the layer will increase from 4 to 14% upon raising the CaP form 10 to 40% of the sample. Upon subsequent attack by acid producing bacteria, this hydroxyapatite layer is likely to re-dissolve releasing a localised highly lethal concentration of CHX [23]. These formulations, therefore, potentially could provide prolonged and localised antibacterial activity at the interface between the restoration and the tooth structure. It has to be mentioned, however, that the biological environment is more complex and the above observations should be tested on a suitable clinical model.

### 4.3. Flexural strength and modulus

Previous work with the formulations in this study has shown the dry strength and modulus decreases by approximately 20% and 50% respectively as the CaP content is raised from 0 to 40% (data submitted for publication). This is not due to changes in levels of cure but possibly caused by a lack of coupling agent between CaP fillers and polymer matrix phase. The above work (Table 1) shows additionally greater decline in strength and modulus is observed with higher CaP. This may be a consequence of increased water sorption. Furthermore, there may be increasing porosity due to greater release of some unreacted MCPM to promote mineralisation. Commercial composites have been shown to have initial flexural strength between 100 to 180 MPa [49] but they can decline by more than 100% after storing in water for 12 months [50]. In 1 month a typical decline would be ~10–20%. The strengths observed for the experimental materials therefore at 1 month are still well within the range obtained with commercial composites. Whilst a decrease in strength is disadvantageous, decrease in modulus will increase resilience and energy absorption [51].

## 5. Conclusion

In this study, various quantitative methods for monitoring HA precipitation kinetics on composite surfaces were introduced. Incorporating calcium phosphates in the form of reactive MCPM and β-TCP into dental composites promoted precipitation of HA in SBF. HA precipitation mass was proportional to the CaP content as were parameters obtained from EDAX and Raman studies of the composite surfaces. The above study suggested that most of the ions forming the surface HA were released from within the material. Antibacterial CHX was found to be bound to the HA precipitate at high concentration and at 12 weeks made up to 15 wt.% of the HA layer. The strength of the materials decreased linearly upon raising CaP levels. The lowest value, however, was well above 100 MPa, giving the materials competitive strength compared to commercial composites. In conclusion, these materials could potentially solve the problem of microleakage and recurrent carries as well as promote remineralisation of demineralised dentine.

## Conflicts of interest

The use of reactive fillers in dental composites is covered by a patent of the corresponding author.

## Acknowledgements

EPSRC (project EP/I022341/1), Davis Schottlander & Davis Ltd. and the Libyan government provided financial support. ESSCHEM, Himed and Ozics supplied monomers, CaP and silica fillers, respectively. George Georgiou, Nicola Mordan and Graham Palmer provided technical support.

## References

[1] P.S. Stein, J. Sullivan, J.E. Haubenreich, P.B. Osborne, Composite resin in medicine and dentistry, J. Long-Term Eff. Med. Implants 15 (2005) 641–654.
[2] S. Rüttermann, S. Krüger, W.H.-M. Raab, R. Janda, Polymerization shrinkage and hygroscopic expansion of contemporary posterior resin-based filling materials—a comparative study, J. Dent. 35 (2007) 806–813.
[3] D.C. Sarrett, Clinical challenges and the relevance of materials testing for posterior composite restorations, Dent. Mater. 21 (2005) 9–20.
[4] T. Beazoglou, S. Eklund, D. Heffley, J. Meiers, L.J. Brown, H. Bailit, Economic impact of regulating the use of amalgam restorations, Public Health Rep. 122 (2007) 657.
[5] X. Wu, Y. Sun, W. Xie, Y. Liu, X. Song, Development of novel dental nanocomposites reinforced with polyhedral oligomeric silsesquioxane (POSS), Dent. Mater. 26 (2010) 456–462.
[6] H. Fong, Electrospun nylon 6 nanofiber reinforced BIS-GMA/TEGDMA dental restorative composite resins, Polymer 45 (2004) 2427–2432.
[7] M. Hosseinalipour, J. Javadpour, H. Rezaie, T. Dadras, A.N. Hayati, Investigation of mechanical properties of experimental Bis-GMA/TEGDMA dental composite resins containing various mass fractions of silica nanoparticles, J. Prosthodont. 19 (2010) 112–117.
[8] M.-H. Chen, Update on dental nanocomposites, J. Dent. Res. 89 (2010) 549–560.
[9] R.W. Arcís, A. López-Macipe, M. Toledano, E. Osorio, R. Rodríguez-Clemente, J. Murtra, et al., Mechanical properties of visible light-cured resins reinforced with hydroxyapatite for dental restoration, Dent. Mater. 18 (2002) 49–57.
[10] C. Domingo, R. Arcís, E. Osorio, R. Osorio, M.A. Fanovich, R. Rodríguez-Clemente, et al., Hydrolytic stability of experimental hydroxyapatite-filled dental composite materials, Dent. Mater. 19 (2003) 478–486.
[11] C. Santos, R. Clarke, M. Braden, F. Guitian, K. Davy, Water absorption characteristics of dental composites incorporating hydroxyapatite filler, Biomaterials 23 (2002) 1897–1904.

[12] D. Skrtic, J.M. Antonucci, Effect of bifunctional comonomers on mechanical strength and water sorption of amorphous calcium phosphate-and silanized glass-filled Bis-GMA-based composites, Biomaterials 24 (2003) 2881–2888.
[13] D. Skrtic, J. Antonucci, Dental composites based on amorphous calcium phosphate—resin composition/physicochemical properties study, J. Biomater. Appl. 21 (2007) 375–393.
[14] D. Skrtic, J.M. Antonucci, E.D. Eanes, Improved properties of amorphous calcium phosphate fillers in remineralizing resin composites, Dent. Mater. 12 (1996) 295–301.
[15] D. Skrtic, J. Antonucci, E. Eanes, N. Eidelman, Dental composites based on hybrid and surface-modified amorphous calcium phosphates, Biomaterials 25 (2004) 1141–1150.
[16] H.H. Xu, M.D. Weir, L. Sun, Calcium and phosphate ion releasing composite: effect of pH on release and mechanical properties, Dent. Mater. 25 (2009) 535–542.
[17] H.H. Xu, L. Sun, M.D. Weir, S. Takagi, L.C. Chow, B. Hockey, Effects of incorporating nanosized calcium phosphate particles on properties of whisker-reinforced dental composites, J. Biomed. Mater. Res. B Appl. Biomater. 81 (2007) 116–125.
[18] H. Xu, L. Sun, M. Weir, J. Antonucci, S. Takagi, L. Chow, et al., Nano DCPA-whisker composites with high strength and Ca and PO4 release, J. Dent. Res. 85 (2006) 722–727.
[19] H.H. Xu, J.L. Moreau, L. Sun, L.C. Chow, Strength and fluoride release characteristics of a calcium fluoride based dental nanocomposite, Biomaterials 29 (2008) 4261–4267.
[20] H. Xu, M. Weir, L. Sun, J. Moreau, S. Takagi, L. Chow, et al., Strong nanocomposites with Ca, PO4, and F release for caries inhibition, J. Dent. Res. 89 (2010) 19–28.
[21] D. Skrtic, J.M. Antonucci, E.D. Eanes, F.C. Eichmiller, G.E. Schumacher, Physicochemical evaluation of bioactive polymeric composites based on hybrid amorphous calcium phosphates, J. Biomed. Mater. Res. 53 (2000) 381–391.
[22] I. Mehdawi, E.A.A. Neel, S.P. Valappil, G. Palmer, V. Salih, J. Pratten, et al., Development of remineralizing, antibacterial dental materials, Acta Biomater. 5 (2009) 2525–2539.
[23] I. Mehdawi, J. Pratten, D.A. Spratt, J.C. Knowles, A.M. Young, High strength remineralizing, antibacterial dental composites with reactive calcium phosphates, Dent. Mater. 29 (2013) 473–484.
[24] J.L. Ferracane, Resin composite—state of the art, Dent. Mater. 27 (2011) 29–38.
[25] J. Lööf, F. Svahn, T. Jarmar, H. Engqvist, C.H. Pameijer, A comparative study of the bioactivity of three materials for dental applications, Dent. Mater. 24 (2008) 653–659.
[26] K. Welch, Y. Cai, H. Engqvist, M. Strømme, Dental adhesives with bioactive and on-demand bactericidal properties, Dent. Mater. 26 (2010) 491–499.
[27] H. Engqvist, J.-E. Schultz-Walz, J. Loof, G.A. Botton, D. Mayer, M.W. Phaneuf, et al., Chemical and biological integration of a mouldable bioactive ceramic material capable of forming apatite in vivo in teeth, Biomaterials 25 (2004) 2781–2787.
[28] M.G. Gandolfi, P. Taddei, F. Siboni, E. Modena, E.D. De Stefano, C. Prati, Biomimetic remineralization of human dentin using promising innovative calcium–silicate hybrid “smart” materials, Dent. Mater. 27 (2011) 1055–1069.
[29] S.R. Paital, N.B. Dahotre, Wettability and kinetics of hydroxyapatite precipitation on a laser-textured Ca–P bioceramic coating, Acta Biomater. 5 (2009) 2763–2772.
[30] X. Lu, Y. Leng, Theoretical analysis of calcium phosphate precipitation in simulated body fluid, Biomaterials 26 (2005) 1097–1108.
[31] E.V. Pecheva, L.D. Pramatarova, M.F. Maitz, M.T. Pham, A.V. Kondyuirin, Kinetics of hydroxyapatite deposition on solid substrates modified by sequential implantation of Ca and P ions: part I. FTIR and Raman spectroscopy study, Appl. Surf. Sci. 235 (2004) 176–181.
[32] E.V. Pecheva, L.D. Pramatarova, M.F. Maitz, M.T. Pham, A.V. Kondyuirin, Kinetics of hydroxyapatite deposition on solid substrates modified by sequential implantation of Ca and P ions: part II: morphological, composition and structure study, Appl. Surf. Sci. 235 (2004) 170–175.
[33] H. Xu, J. Moreau, L. Sun, L. Chow, Novel CaF2 nanocomposite with high strength and fluoride ion release, J. Dent. Res. 89 (2010) 739–745.
[34] D. Leung, D.A. Spratt, J. Pratten, K. Gulabivala, N.J. Mordan, A.M. Young, Chlorhexidine-releasing methacrylate dental composite materials, Biomaterials 26 (2005) 7145–7153.
[35] A. Wiegand, W. Buchalla, T. Attin, Review on fluoride-releasing restorative materials—fluoride release and uptake characteristics, antibacterial activity and influence on caries formation, Dent. Mater. 23 (2007) 343–362.
[36] R. Gendron, D. Grenier, T. Sorsa, D. Mayrand, Inhibition of the activities of matrix metalloproteinases 2, 8, and 9 by chlorhexidine, Clin. Diagn. Lab. Immunol. 6 (1999) 437–439.
[37] C. Splieth, M. Rosin, B. Gellissen, Determination of residual dentine caries after conventional mechanical and chemomechanical caries removal with Carisolv, Clin. Oral Investig. 5 (2001) 250–253.
[38] D. Misra, Interaction of chlorhexidine digluconate with and adsorption of chlorhexidine on hydroxyapatite, J. Biomed. Mater. Res. 28 (1994) 1375–1381.
[39] R.K. Brundavanam, G.E.J. Poinern, D. Fawcett, Modelling the crystal structure of a 30 nm sized particle based hydroxyapatite powder synthesised under the influence of ultrasound irradiation from X-ray powder diffraction data, Am. J. Mater. Sci. 3 (2013) 84–90.
[40] C. Santos, Z. Luklinska, R. Clarke, K. Davy, Hydroxyapatite as a filler for dental composite materials: mechanical properties and in vitro bioactivity of composites, J. Mater. Sci. Mater. Med. 12 (2001) 565–573.
[41] X. Wang, H. Sun, J. Chang, Characterization of Ca3SiO5/CaCl2 composite cement for dental application, Dent. Mater. 24 (2008) 74–82.
[42] J. Liu, Y. Shirosaki, T. Miyazaki, Bioactive polymethylmethacrylate bone cement modified with combinations of phosphate group-containing monomers and calcium acetate, J. Biomater. Appl. 29 (9) (2015) 1296–1303.
[43] M. Bohner, Calcium orthophosphates in medicine: from ceramics to calcium phosphate cements, Injury 31 (2000) D37–D47.
[44] M.H. Santos, O. Md, S. LPdF, H.S. Mansur, W.L. Vasconcelos, Synthesis control and characterization of hydroxyapatite prepared by wet precipitation process, Mater. Res. 7 (2004) 625–630.
[45] K. Anusavice, N.-Z. Zhang, C. Shen, Controlled release of chlorhexidine from UDMA-TEGDMA resin, J. Dent. Res. 85 (2006) 950–954.
[46] G. Palmer, F.H. Jones, R.W. Billington, G.J. Pearson, Chlorhexidine release from an experimental glass ionomer cement, Biomaterials 25 (2004) 5423–5431.
[47] L. Cheng, M.D. Weir, H.H.K. Xu, A.M. Kraigsley, N.J. Lin, S. Lin-Gibson, et al., Antibacterial and physical properties of calcium–phosphate and calcium–fluoride nanocomposites with chlorhexidine, Dent. Mater. 28 (2012) 573–583.
[48] W. Xia, M.M. Razi, P. Ashley, E.A. Neel, M. Hofmann, A. Young, Quantifying effects of interactions between polyacrylic acid and chlorhexidine in dicalcium phosphate-forming cements, J. Mater. Chem. B 2 (2014) 1673–1680.
[49] L.C. Boaro, F. Gonçalves, T.C. Guimarães, J.L. Ferracane, C.S. Pfeifer, R.R. Braga, Sorption, solubility, shrinkage and mechanical properties of “low-shrinkage” commercial resin composites, Dent. Mater. 29 (2013) 398–404.
[50] A. Curtis, A. Shortall, P. Marquis, W. Palin, Water uptake and strength characteristics of a nanofilled resin-based composite, J. Dent. 36 (2008) 186–193.
[51] A. Aljabo, W. Xia, S. Liaqat, M.A. Khan, J.C. Knowles, P. Ashley, A.M. Young, Conversion, shrinkage, water sorption, flexural strength and modulus of re-mineralizing dental composites, Dent. Mater. 31 (2015) 1279–1289.